THE ASTROPHYSICAL JOURNAL SUPPLEMENT SERIES, 86:389–400, 1993 June

N-BODY REALIZATIONS OF COMPOUND GALAXIES

LARS HERNQUIST[1]
Board of Studies in Astronomy and Astrophysics, Santa Cruz, CA 95064; E-mail: lars@helios.ucsc.edu
Received 1992 September 23; accepted 1992 December 4

ABSTRACT

A prescription for constructing *N*-body models of galaxies consisting of more than one component is described. Spatial density profiles are realized exactly, but the phase space distribution is approximated using moments of the collisionless Boltzmann equation. While this approach is not fully rigorous, empirical tests suggest that it is adequate for studies of, e.g., interacting galaxies and the forced response of galaxies to imposed perturbations such as bars.

Subject headings: galaxies: interactions — galaxies: structure — methods: numerical

1. INTRODUCTION

Early dynamical studies of galaxy evolution and formation typically considered the self-consistent behavior of only one component; e.g., the dark matter believed to dominate the overall mass distribution or disks like those in real spirals. Observationally, it is quite clear, however, that galaxies are composite objects and include several distinct, but interacting parts. For example, spirals, like the Milky Way, comprise dark matter halos, luminous disks and bulges, and small amounts of interstellar gas.

Generating initial conditions for numerical experiments of galaxy formation in a hierarchical universe is a well-defined procedure: particle coordinates are obtained from the cosmological perturbation spectrum evolved according to linear theory (e.g., Efstathiou et al. 1985; Dubinski & Carlberg 1991). By contrast, the optimal procedure for constructing already formed galaxies for, e.g., scattering experiments is problematic. Of course, if the distribution function were known, creating individual galaxies would be trivial. Unfortunately, this is almost never the case, except in highly idealized situations, and some alternate procedure must be employed.

One possibility is to model only selected components of a galaxy and represent the others by rigid potentials, making some simplifying approximations about the nature of the distribution function, as in restricted three-body methods (e.g., Toomre & Toomre 1972; Hernquist & Quinn 1988). These techniques do not allow for the self-consistent interaction among the various components, however. Recent simulations suggest that transfer of angular momentum and binding energy between, e.g., dark and luminous matter (Barnes 1988, 1992; Hernquist 1992; Hernquist & Weinberg 1992), gas and collisionless matter (Hernquist 1989, 1991; Barnes & Hernquist 1991; Hernquist & Barnes 1991), and between disks and bulges (Barnes 1988, 1992; Hernquist 1993) plays a critical role in determining the long-term structure of galaxies perturbed by tidal forces and bars. Clearly, simulations which are not fully self-consistent are inadequate to address detailed issues concerning the structure of remnants.

One scheme for constructing *N*-body models of galaxies consisting of bulges, disks, and halos has been pioneered by Barnes (1988, 1992). In his approach, bulges and halos are first realized with particles and allowed to relax, numerically, in each others' presence. Once the spheroid has neared equilibrium, the gravitational field of a disk is imposed on it, and the bulge and halo are evolved further until they are again near equilibrium. Finally, the disk component is realized with particles whose velocity distribution function is approximated with moments of the collisionless Boltzmann equation (hereafter, CBE).

Barnes' method has the virtue of simplicity and has been used extensively to study major mergers without (Barnes 1988, 1992) and with gas (Barnes & Hernquist 1991, 1992; Hernquist & Barnes 1991), and the response of large spirals to small tidal perturbations (Hernquist 1990a). Unfortunately, this scheme is rather limited since the galaxy is modified by the numerical procedure used to force the model toward equilibrium. Thus, it is not possible to arbitrarily specify the parameters defining the structure of the various components in the equilibrium model without iterating. Since the "pre-evolution" phase is costly, this option is prohibitive in situations where a systematic coverage of parameter space is desired. In view of the fact that some aspects of galaxy evolution appear to be driven, for example, by the detailed shape of the rotation curve, some other technique must be found which makes it possible to vary the structure parameters in a more systematic fashion.

This paper describes one such approach. Essentially, the method described here generalizes that employed by previous workers to construct self-consistent disk models (e.g., Hernquist & Quinn 1989; Hernquist 1989; Quinn, Hernquist, & Fullager 1993; Barnes 1988, 1992) by approximating the distribution function for *all* components using moments of the CBE. This technique is not rigorous, of course, since the velocity field is not exactly that which would be obtained from the distribution function, if it were known. However, as demonstrated by the empirical tests here, the models thus constructed are nearly in equilibrium and evolve negligibly (for many applications) in isolation. Thus, it is now possible to generate compound galaxies with systematic variations in their internal structure.

[1] Alfred P. Sloan Foundation Fellow, Presidential Faculty Fellow.

The organization of the paper is as follows: The prescription used to construct the galaxies is described in § 2. Empirical tests demonstrating the stability of the approach are presented in § 3. Finally, § 4 notes conclusions.

2. METHOD

In principle, the technique described here can be applied to any axisymmetric mass profile whose distribution function depends on two integrals of motion or when the moment equations of the CBE can be simplified using epicyclic theory, as for thin disks supported mostly by rotation. As a specific example, the ensuing discussion considers models of spiral galaxies consisting of self-gravitating disks, bulges, and halos.

2.1. *Density Profiles*

Observations of our galaxy and external spirals suggest that their disk components are reasonably well fitted by profiles which decay exponentially with cylindrical radius (Freeman 1970) and which are described by isothermal sheets perpendicular to the disk plane (Bahcall & Soneira 1980; Spitzer 1942). A concise form for the distribution of disk material is thus given by

$$\rho_d(R, z) = \frac{M_d}{4\pi h^2 z_0} \exp(-R/h) \operatorname{sech}^2\left(\frac{z}{z_0}\right), \quad (2.1)$$

where M_d is the disk mass, h is a radial scale length, and z_0 is a vertical scale thickness. This choice is to some extent arbitrary and other vertical or radial functional forms could be employed if desired.

The exact spatial distribution of dark matter around galaxies is unknown, but observations of rotation curves of external spirals imply that halos are characterized by isothermal spheres over some radial interval. For simplicity, the following phenomenological density profile is used to represent halos in the present study:

$$\rho_h(r) = \frac{M_h}{2\pi^{3/2}} \frac{\alpha}{r_c} \frac{\exp(-r^2/r_c^2)}{r^2 + \gamma^2}, \quad (2.2)$$

where M_h is the halo mass, r_c is a cutoff radius, and γ is a core radius. The normalization constant α is defined by

$$\alpha = \{1 - \sqrt{\pi} q \exp(q^2)[1 - \operatorname{erf}(q)]\}^{-1}, \quad (2.3)$$

where $q = \gamma/r_c$. Halos are truncated at what are likely artificially small radii to reduce the computational task of integrating loosely bound particles that do not affect the structure of the more tightly bound luminous components. The cumulative mass profile, $M_h(r)$, and potential, $\Phi_h(r)$, corresponding to $\rho_h(r)$ are

$$M_h(r) = \frac{2M_h\alpha}{\sqrt{\pi}} \int_0^{r/r_c} \frac{x^2 \exp(-x^2)}{x^2 + q^2}\, dx, \quad (2.4)$$

$$\Phi_h(r) = -\frac{GM_h(r)}{r} + \frac{GM_h\alpha}{\sqrt{\pi} r_c} \operatorname{Ei}\left[-\left(\frac{r}{r_c}\right)^2 - q^2\right], \quad (2.5)$$

where Ei (z) is an exponential integral (e.g., Gradshteyn & Ryzhik 1980).

Bulges are modeled by an oblate generalization of the potential-density pair proposed by Hernquist (1990b) for spherical galaxies and bulges. Namely, the bulge density profile is

$$\rho_b(m) = \frac{M_b}{2\pi a^2} \frac{1}{m(1+m)^3}, \quad (2.6)$$

where M_b is the bulge mass, a is a scale length along the major axis, c is a scale length along the minor axis, and

$$m^2 = \frac{x^2 + y^2}{a^2} + \frac{z^2}{c^2} \quad (2.7)$$

(e.g., Dubinski & Carlberg 1991). The cumulative mass profile and potential corresponding to $\rho_b(m)$ can be written

$$M_b(m) = M_b \frac{m^2}{(1+m)^2}, \quad (2.8)$$

$$\Phi_b(\mathbf{r}) = -\frac{GM_b}{2} \int_0^\infty \frac{du}{\Delta(u)} \frac{1}{[1 + m(u)]^2}, \quad (2.9)$$

where

$$\Delta(u) = (a^2 + u)\sqrt{c^2 + u}, \quad (2.10)$$

$$m^2(u) = \frac{R^2}{a^2 + u} + \frac{z^2}{c^2 + u}. \quad (2.11)$$

Once the density structure of the various components is defined, as by equations (2.1), (2.2), and (2.6), and the relevant parameters are specified, particle coordinates can be initialized trivially using a variety of techniques (e.g., Press et al. 1986). In so doing, it is expedient to represent the different parts with unequal-mass particles to mitigate effects of discreteness noise in the low-mass components.

2.2. *Velocity Structure*

Once realized with particles according to relations like those in § 2.1, the density structure of the model is exactly specified. If the distribution function were known, particle velocities could be initialized in like manner and the initial conditions would be fully determined. This is certainly not possible for density profiles like those discussed above. Alternatively, some progress can be made by recognizing that the density structure by itself determines the lowest order moments of the CBE. A simple method for initializing particle velocities is thus provided by computing some of these moments and approximating the distribution function in velocity space by forms having these moments. This scheme is approximate in that the moment hierarchy must be truncated at low order. Nevertheless, it is relatively straightforward to implement and can be made increasingly precise by including more and more moments. Furthermore, it easily generalizes to a variety of nonspherical mass profiles, allows compound objects to be realized by treating some components as external potentials, and in certain cases directly incorporates the effect of force softening.

The method will be illustrated here with a fairly crude, but effective implementation applied to disk-bulge-halo galaxies as described in § 2.1. Consider first the halo component, which is conceptually the simplest in cases where it dominates the overall potential.

2.2.1. *Halos*

If the mass distribution were spherical, the second moment of the CBE for the halo would read

$$\frac{d(\rho_h\overline{v_r^2})}{dr} + \frac{\rho_h}{r}[2\overline{v_r^2} - (\overline{v_\theta^2} + \overline{v_\phi^2})] = -\rho_h \frac{d\Phi}{dr}, \quad (2.12)$$

where $\overline{v_r^2}$, $\overline{v_\theta^2}$, and $\overline{v_\phi^2}$, are the dispersions in spherical coordinates (e.g., Binney & Tremaine 1987). If the model is also isotropic, equation (2.12) can be integrated to give

$$\overline{v_r^2} = \frac{1}{\rho_h(r)} \int_r^\infty \rho_h(r) \frac{d\Phi}{dr} dr. \quad (2.13)$$

Here, Φ includes not only the self-gravity of the halo but the contributions of the other components to the gravitational field as well. In what follows, it is useful to rewrite equation (2.13) in the form

$$\overline{v_r^2} = \frac{1}{\rho_h(r)} \int_r^\infty \rho_h(r) \frac{GM(r)}{r^2} dr, \quad (2.14)$$

where $M(r)$ is the cumulative mass distribution.

The radial dispersion can now be computed as a function of radius using the known analytic form for $\rho_h(r)$ and by binning the mass in spherical shells to evaluate the integral in equation (2.14) numerically. Force softening is trivially included by distributing the mass of each particle over several radial bins according to the value of the softening length. The next step is to select a function whose second moment is $\overline{v_r^2}$; an obvious choice is simply a Gaussian. In practice, it is expedient to select *speeds* of particles from

$$F(v, r) = 4\pi\left(\frac{1}{2\pi\sigma^2}\right)^{3/2} v^2 \exp(-v^2/2\overline{v_r^2}), \quad (2.15)$$

where $F(v, r)$ is normalized so that

$$\int_0^\infty F(v, r)dv = 1.$$

Once the speed of a halo particle has been chosen, the Cartesian velocity components are initialized from v, assuming isotropy.

The approach just described has two defects. First, the choice of $F(v, r)$ in equation (2.15) is an approximation. The initialization procedure can be made more accurate by computing higher order moments and selecting more general forms for $F(v, r)$. Empirical tests suggest that the second moment alone is adequate, provided that the speed is limited at a given radius to some fraction of the local escape speed. Good results were obtained by requiring $v \le 0.95v_{esc}$.

Second, the potential of a composite disk-bulge-halo galaxy is not spherical at small radii owing mainly to the contribution of the disk. In principle, this problem can be mitigated using a variant of the procedure described below for initializing nonspherical bulges. Numerical tests suggest, however, that for many applications it is adequate to bin the disk and bulge components in *spherical* shells as long as the halo dominates the mass distribution, since the quadrupole component of the potential declines rapidly with radius. This does, however, result in a minor redistribution of halo mass near the center of the galaxy once it is allowed to evolve dynamically. Empirically, it was found that this redistribution could be practically eliminated by arbitrarily contracting the disk in radius by $\approx$35% when binning its contribution to the cumulative mass profile in equation (2.14).

2.2.2. *Bulges*

Observations of bulges in external galaxies and the Milky Way imply that they are nonspherical and are flattened partly by rotation (e.g., Illingworth & Schechter 1982; Kormendy 1982; Kormendy & Illingworth 1982; Minniti et al. 1992). The procedure used to realize nonspherical bulges is similar to that described above for halos, but generalized to axisymmetric systems.

For an axisymmetric model, the velocity dispersion is not isotropic and has cylindrical components

$$\overline{v_R^2} = \overline{v_z^2} = \frac{1}{\rho(\psi, R)} \int_0^\psi \rho(\psi, R)d\psi, \quad (2.16)$$

$$\sigma_\phi^2 = \overline{v_R^2} + \frac{1}{\rho(\psi, R)} \int_0^\psi R \frac{\partial\rho(\psi, R)}{\partial R} d\psi, \quad (2.17)$$

where $\psi = -\Phi$ (de Zeeuw 1987; Dejonghe 1986).

In the spirit of the approximations described in § 2.2.1, a simple first attempt is to treat the halo and disk contributions to the dispersion of the bulge as spherical and isotropic, but to include the nonspherical nature of the bulge's self-gravity using equations (2.16) and (2.17). In that case, the cylindrical components of the dispersion can be written

$$\overline{v_i^2} = \overline{v_{i,\text{bulge}}^2} + \overline{v_{r,\text{disk+halo}}^2}, \quad (2.18)$$

for $i \equiv R$ and z, along with a similar relation for σ_ϕ^2, where $\overline{v_{i,\text{bulge}}^2}$ incorporates the bulge self-gravity using equations (2.16) and (2.17), and $\overline{v_{r,\text{disk+halo}}^2}$ represents the isotropic dispersion of the bulge particles in the spherically averaged halo and disk potential, computed in a manner similar to that described in § 2.2.1. Once the full dispersions have been computed for each bulge particle, the velocities can be initialized by drawing from Gaussians with these dispersions, limiting the total speed to the local escape speed. Rotation can be included simply by requiring all particles to circulate in the same sense around the symmetry axis of the model.

Implementation of this procedure is complicated by a number of technical details; in particular, the need to evaluate the integrals appearing in equations (2.16) and (2.17) numerically. For each particle, the upper limit of integration is determined from the value of ψ appropriate for its spatial coordi-

nates, as computed from equation (2.9). In evaluating integrals like that in equation (2.9), it is expedient to split the integration into two parts, one ranging from [0, 1] and the other spanning [1, ∞), and changing variables in the second integral by $u = 1/w^6$.

Once the upper limit is known, the integrals in equations (2.16) and (2.17) can be computed numerically as follows. At each point along the path of integration, R and ψ are known. Equation (2.9), which gives $\Phi(R, z)$ can be inverted numerically by Newton-Raphson iteration to give $z = z(R, \psi)$. Equation (2.6) can then be used to compute $\rho = \rho(R, \psi)$. For the integral in equation (2.17), it is useful to write

$$\left.\frac{\partial \rho}{\partial R}\right|_{\psi} = \left.\frac{\partial \rho}{\partial R}\right|_{z} + \left.\frac{\partial \rho}{\partial z}\right|_{R} \left.\frac{\partial z}{\partial R}\right|_{\psi} . \tag{2.19}$$

The partial derivatives of ρ with respect to z and R can be obtained analytically from equation (2.6). The final partial derivative in equation (2.19) can be calculated from

$$\left.\frac{\partial z}{\partial R}\right|_{\psi} = -\frac{\partial \psi/\partial R|_{z}}{\partial \psi/\partial z|_{R}} . \tag{2.20}$$

The partial derivatives of ψ in equation (2.20) can be computed by differentiating equation (2.9) analytically and then evaluating the resulting integrals numerically, dividing the range of integration into two parts, as noted above.

2.2.3. *Disks*

The strategy employed to realize the disk components of the galaxies is similar to that described by Quinn et al. (1993); salient features are summarized here for completeness. The objective is to construct disks having the density structure of, e.g., equation (2.1) so that the vertical scale thickness, z_0, is constant with cylindrical radius. In specifying the velocity structure of the disk, it is necessary to constrain the shape of the velocity ellipsoid and some measure of how cold the disk is dynamically. These various conditions can be imposed again using moment equations of the CBE, as above, but supplemented by constraints from observations of disk galaxies.

In the notation employed by Binney & Tremaine (1987), the velocity structure of a thin disk in cylindrical coordinates is approximately determined by the lowest order moments $\overline{v_R^2}$, $\overline{v_z^2}$, σ_ϕ^2, and $\overline{v_\phi}$ which are, respectively, the radial, vertical, and azimuthal dispersions, and the azimuthal streaming velocity. Observations of external disk galaxies (Lewis & Freeman 1989; van der Kruit & Searle 1981) suggest that the radial dispersion is proportional to the radial surface density, implying that $\overline{v_R^2}$ scales roughly as

$$\overline{v_R^2} \propto \exp(-R/h) . \tag{2.21}$$

For an isothermal sheet, the vertical dispersion in the midplane is also simply related to the disk surface density, $\Sigma(R)$, by

$$\overline{v_z^2} = \pi G \Sigma(R) z_0 . \tag{2.22}$$

Hence, for these choices, $\overline{v_R^2} \propto \overline{v_z^2}$, so that the ratio of radial to vertical dispersions is constant throughout the disk.

The radial and vertical velocity structure in the disk plane are determined by equations (2.21) and (2.22) once the normalization constant in equation (2.21) is specified. In the present context, it is convenient to fix this factor by prescribing the Toomre Q parameter (Toomre 1963) at a particular location in the disk. For a stellar disk the critical radial dispersion for axisymmetric stability is given by

$$\sigma_R|_{\rm crit} = \frac{3.36 G \Sigma}{\kappa} , \tag{2.23}$$

where κ is the epicyclic frequency, defined by

$$\kappa^2 = \frac{3}{R}\frac{\partial \Phi}{\partial R} + \frac{\partial^2 \Phi}{\partial R^2} . \tag{2.24}$$

In the implementation here, the radial dispersion in equation (2.21) is normalized by requiring it to be a multiple Q of the critical dispersion at some reference point in the disk, $R_{\rm ref}$; typically, $R_{\rm ref} \sim 2$–$3h$. This is accomplished by evaluating κ and Σ for all particles within a narrow annulus centered on $R_{\rm ref}$ and using them to compute a mean value for $Q * \sigma_R|_{\rm crit}$ in the neighborhood of $R_{\rm ref}$. In calculating κ, the contribution to the potential and force fields from *all* components is included.

Finally, it is necessary to compute the azimuthal moments of the disk's velocity field. The relevant second moment of the CBE is

$$\sigma_\phi^2 - \overline{v_R^2} - \frac{R}{\Sigma}\frac{\partial(\Sigma \overline{v_R^2})}{\partial R} - R\frac{\partial(\overline{v_R v_z})}{\partial z} = v_c^2 - \overline{v_\phi}^2 \tag{2.25}$$

(e.g., Binney & Tremaine 1987). For simplicity, the azimuthal dispersion is chosen to be related to the radial dispersion via the epicyclic approximation

$$\sigma_\phi^2 = \overline{v_R^2}\frac{\kappa^2}{4\Omega^2} , \tag{2.26}$$

where Ω is the angular frequency, computed from the potential. This relation, along with equations (2.21) and (2.22) fully specify the shape of the velocity ellipsoid in the disk plane. For an exponential surface density profile, as assumed here, equation (2.25) can be rewritten as

$$\overline{v_\phi}^2 - v_c^2 = \overline{v_R^2}\left[1 - \frac{\kappa^2}{4\Omega^2} - \frac{R}{h} + \frac{\partial(\ln \overline{v_R^2})}{\partial \ln R} + \frac{R}{\overline{v_R^2}}\frac{\partial(\overline{v_R v_z})}{\partial z}\right] , \tag{2.27}$$

using equation (2.26). Contrary to assertions made by Quinn et al. (1993), the final term in equation (2.27) is problematic since it depends on the orientation of the velocity ellipsoid away from the disk plane. In the simplest case, the velocity ellipsoid remains aligned with the coordinate axes and this term vanishes. In that event, assuming an exponential distribution for the radial velocity dispersion, equation (2.27) simplifies to

$$\overline{v_\phi}^2 - v_c^2 = \overline{v_R^2}\left(1 - \frac{\kappa^2}{4\Omega^2} - 2\frac{R}{h}\right) . \tag{2.28}$$

Once $\overline{v_R^2}$, κ, and Ω have been calculated, the azimuthal dispersion and streaming velocity can be computed for each particle using equations (2.26) and (2.28). As discovered by Quinn et al. (1993), however, the approximations underlying these relations can break down near the center of the galaxy; in particular, equation (2.28) can, in certain cases, produce imaginary v_ϕ at small radii. It was determined that the difficulty lies with the term involving the derivative of $\overline{v_R^2}$ in equation (2.27) rising too rapidly as $R \to 0$. The nature of the dispersion of disks near their centers is not well understood, either observationally or theoretically. As suggested by Quinn et al. a possible "fix" is to reduce $\overline{v_R^2}$ at small radii. The detailed form of this reduction is arbitrary; a convenient choice is to "soften" $\overline{v_R^2}$ according to

$$\overline{v_R^2} \propto \exp\left(-\sqrt{R^2 + 2a_s^2}/h\right), \qquad (2.29)$$

where the scale length a_s is taken to be the radius at which $\overline{v_\phi}$ becomes imaginary if it is computed by equation (2.28). A similar reduction factor is also applied to $\overline{v_z^2}$ so that the ratio of vertical to radial dispersions is always constant. Empirical tests indicate that values $a_s \sim h/4$ typically eliminate the difficulty just described in situations where it arises.

With the first and second moments specified, disk velocities are initialized by (1) drawing v_z from a Gaussian distribution with dispersion $\sqrt{\overline{v_z^2}}$; (2) computing v_R by drawing from a Gaussian with dispersion $\sqrt{\overline{v_R^2}}$; (3) determining the random component of the azimuthal velocity by drawing from a Gaussian with dispersion $\sqrt{\sigma_\phi^2}$; (4) computing the azimuthal streaming velocity from the form of equation (2.28) modified by the softening of the radial dispersion, if necessary; and (5) calculating, e.g., the Cartesian velocities in the plane, v_x and v_y, by adding together v_R, the random azimuthal velocity, and $\overline{v_\phi}$.

While somewhat cumbersome, the above procedure suffices to produce stable disks that are nearly in equilibrium in the external potential of the halo and bulge. It is perhaps not too surprising that this approach should yield equilibrium models since the local distribution of velocities in our own Galaxy is well fitted by Gaussians (Schwarzschild 1907; Binney & Tremaine 1987).

3. EMPIRICAL TESTS

The method described in § 2 has been tested in connection with several applications examining the outcomes of galaxy collisions and the structure of merger remnants (Hernquist 1992, 1993; Hernquist & Weil 1993; Hernquist & Bolte 1993). For brevity, the results of these tests will be illustrated with a single model, although others will be discussed where appropriate.

Results are presented in the system of units employed by Hernquist (1992, 1993); namely, the gravitational constant, $G = 1$, the disk exponential scale length, $h = 1$, and the disk mass, $M_d = 1$. Scaled to physical values appropriate for the Milky Way, i.e., $h = 3.5$ kpc and $M_d = 5.6 \times 10^{10}\, M_\odot$, unit time and velocity are 1.31×10^7 yr and 262 km s^{-1}, respectively.

In these units, the galaxy model in the simulation described in detail below has $z_0 = 0.2$, $M_h = 5.8$, $\gamma = 1$, $r_c = 10$, $M_b = 1/3$, $a = 0.2$, and $c = 0.1$. The parameter Q used to normalize the radial velocity dispersion is set to the value 1.5 at a radius similar to that of the solar neighborhood, $R_\odot = 8.5/3.5$. These choices yield a model with properties similar to those of Sb type spirals, like M31.

Some of the properties of the disk in this model are summarized in Figures 1–3. As can be seen from Figure 1, the ratio of radial to critical velocity dispersion for axisymmetric stability has a minimum value $Q \approx 1.5$ near the normalization radius. It rises both inward and outward of this point, but is fairly constant between $1 \lesssim R \lesssim 4$, where most of the disk mass resides. The factor $\Omega - \kappa/2$ is nearly constant except near the center, where it rises rapidly. This behavior is attributable to the shape of the rotation curve and the presence of the compact bulge. Figure 2 shows the three components of disk velocity dispersion in cylindrical coordinates, found by binning and averaging over the particles in the disk. Not surprisingly, the radial and vertical dispersions decay exponentially with radius and the azimuthal dispersion displays similar behavior. The ratio of radial to vertical dispersions is equal to the constant value 1.27 and the ratio of radial to azimuthal dispersions varies between 1.3 and 1.6 for $0 \le R \le 10$. In this case, it was not necessary to "soften" the radial dispersion profile near the center of the disk.

Figure 3 shows the rotation curve of the entire galaxy and the separate contributions to it from the disk, bulge, and halo. The circular speed rises sharply at small radii owing to the bulge contribution. In similar bulgeless models, v_c rises only slowly between $0 \lesssim R \lesssim 2$ (Hernquist 1992). From Figure 3, the rotation period of the disk at its half-mass radius, $R_{1/2} \approx 1.7$, is $\sim T_{1/2} = 11.7$. Scaling to the Milky Way, $T_{1/2} \approx 1.5 \times 10^8$ years.

To check the stability of the initialization procedure described in § 2, a number of N-body realizations of these galaxy models were evolved in isolation. The simulations were performed with a hierarchical tree algorithm (Barnes & Hut 1986), optimized for vector architectures (Hernquist 1990c), with tolerance parameter, $\theta = 0.7$, including quadrupole terms (Hernquist 1987). Forces were softened with a cubic spline (Hernquist & Katz 1989) and disk, bulge, and halo particles had softening lengths $\epsilon_d = 0.08$, $\epsilon_b = 0.06$, and $\epsilon_h = 0.4$, respectively. Equations of motion were integrated using a leap-frog

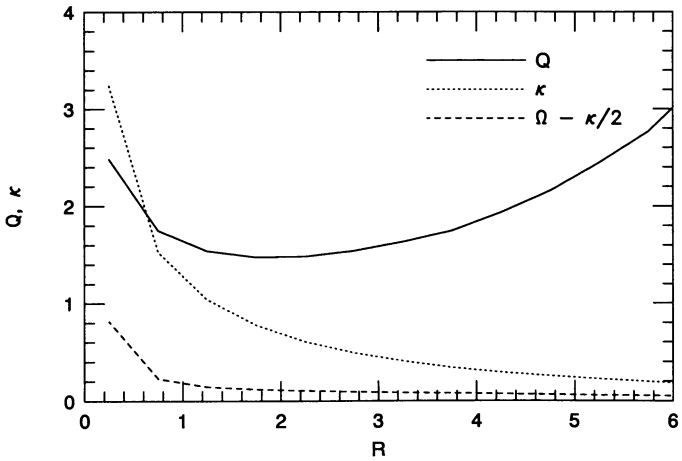

FIG. 1.—Toomre Q parameter, epicyclic frequency, κ, and quantity $\Omega - \kappa/2$ as functions of cylindrical radius for the disk. Values are displayed in the dimensionless system of units described in the text.

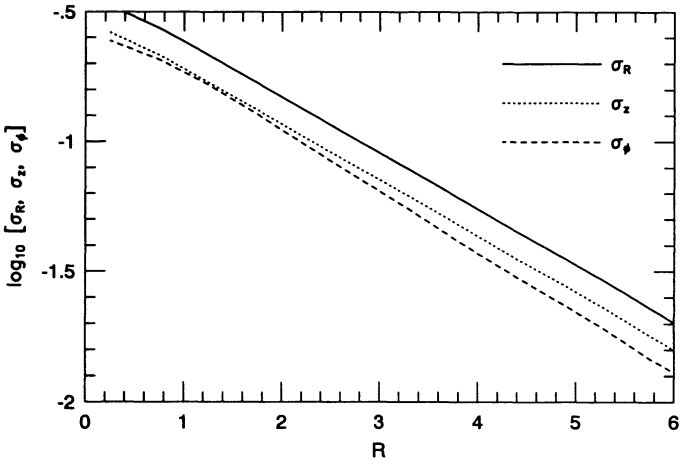

FIG. 2.—Cylindrical components of velocity dispersion of disk vs. cylindrical radius.

algorithm with fixed time step $\Delta t = 0.08$. For these choices, total energy was typically conserved to better than 0.3% and total angular momentum was conserved to better than 0.01%.

Figures 4 and 5 show the time evolution of structure in the disk of one such model. A total of $N = 49,152$ particles were used, with 16,384 in each of the disk, bulge, and halo components. In this simulation, the bulge, although oblate, was initially nonrotating. As is typical of such N-body systems the disk develops some nonaxisymmetric "spiral" features, but is clearly stable in a global sense. This spiral structure likely results from swing amplification of noise in the potential (Toomre 1981), although other instabilities may also be active (Sellwood 1989).

An interesting aside relates to the amplitude of nonaxisymmetric features in the simulations. Disks in models identical to that in Figures 4 and 5 but having *rigid* halos are essentially featureless over these time scales. This implies that much of the spiral structure seen in Figure 4 is a consequence of amplification of noise in the *halo* potential. Unless dark matter halos consist mainly of massive black holes (Lacey & Ostriker 1985) the halo potential in the simulation is certainly much grainier than that in actual galaxies. Clearly, it will not be possible to relate the nonaxisymmetric features in the model disks to observed spiral structure until the level of noise in the potentials of real galaxies is well understood.

Figure 5 shows an edge-on view of the disk. Although mostly quiescent perpendicular to the disk plane, the model displays evidence for weak bending motions during the simulation. Again, similar models with *rigid* halos do not exhibit such features; hence, the bending appears to be driven by discreteness fluctuations in the halo, and their relevance to the structure of real galaxies is problematic.

The bulge and halo components of the galaxy do not evolve dramatically on time scales like those shown in Figures 4 and 5. An example is given in Figure 6, which shows the structure of the bulge from two orthogonal viewing angles at various times during the simulation. If anything, the appearance of the halo is even more static than the bulge. The visual impression given by, e.g., Figure 6 was quantified by computing the moment of inertia tensor for the various components of the galaxy. None display any tendency to evolve significantly immediately following the beginning of the simulation, suggesting that the model is close to equilibrium. On longer time scales, the components evolve slowly, owing to discreteness fluctuations and the appearance of nonaxisymmetric structure in the disk. On time scales like those covered by Figures 4–6, however, such effects are relatively minor.

To support these assertions, the spatial and kinematic structure of each component was monitored during the simulations. An example from this analysis is shown in Figures 7–10, where the volume density of each component is given at $t = 0$ and also at $t = 55$. These mass profiles were obtained by binning the particles in spherical shells for the halo, in ellipsoidal shells for the bulge, in cylinders for the radial distribution of the disk, and in planes for the vertical structure of the disk.

The results presented in Figures 7–10 are quite encouraging. There appears to be almost no evolution in the structure of the various components, aside from slow changes which are not the result of the model being out of equilibrium, but are most likely due to discreteness effects and the growth of nonaxisymmetric features in the disk. Virtually no evolution can be discerned in the halo from Figure 7. Deviations from the exact density structure are consistent with binning errors, aside from the outermost point where the density field is undersampled.

The bulge component exhibits weak evolution near its center, as can be seen by comparing the top and bottom panels of Figure 8. The value $\log m = -0.5$ corresponds to a radius $r \approx 0.06$, which is just the softening length for the bulge particles. In this model, no account was made for softening of the bulge self-gravity. The formalism in § 2.2.2 could be generalized to account for this effect, but it is somewhat of a moot point, since the evolution code cannot resolve structure on these scales. The bulge profile remains impressively close to its initial distribution at larger radii, however, supporting the visual appearance in Figure 6. In particular, the bulge displays no immediate tendency to isotropize.

As can be seen from Figures 9–10, the disk is most prone to evolve over the time scales covered by the simulation. Much of the structural change appears to be driven by the "spiral" features apparent in Figure 4. Vertically, the disk inflates slowly, owing to discreteness effects.

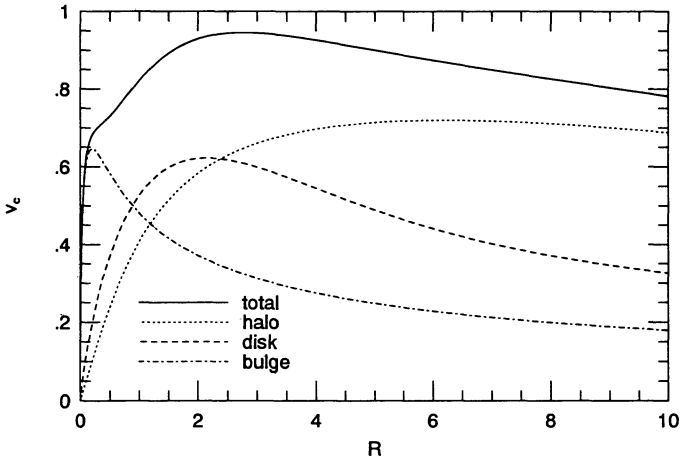

FIG. 3.—Circular speed of galaxy model and separate contributions from disk, bulge, and halo vs. cylindrical radius.

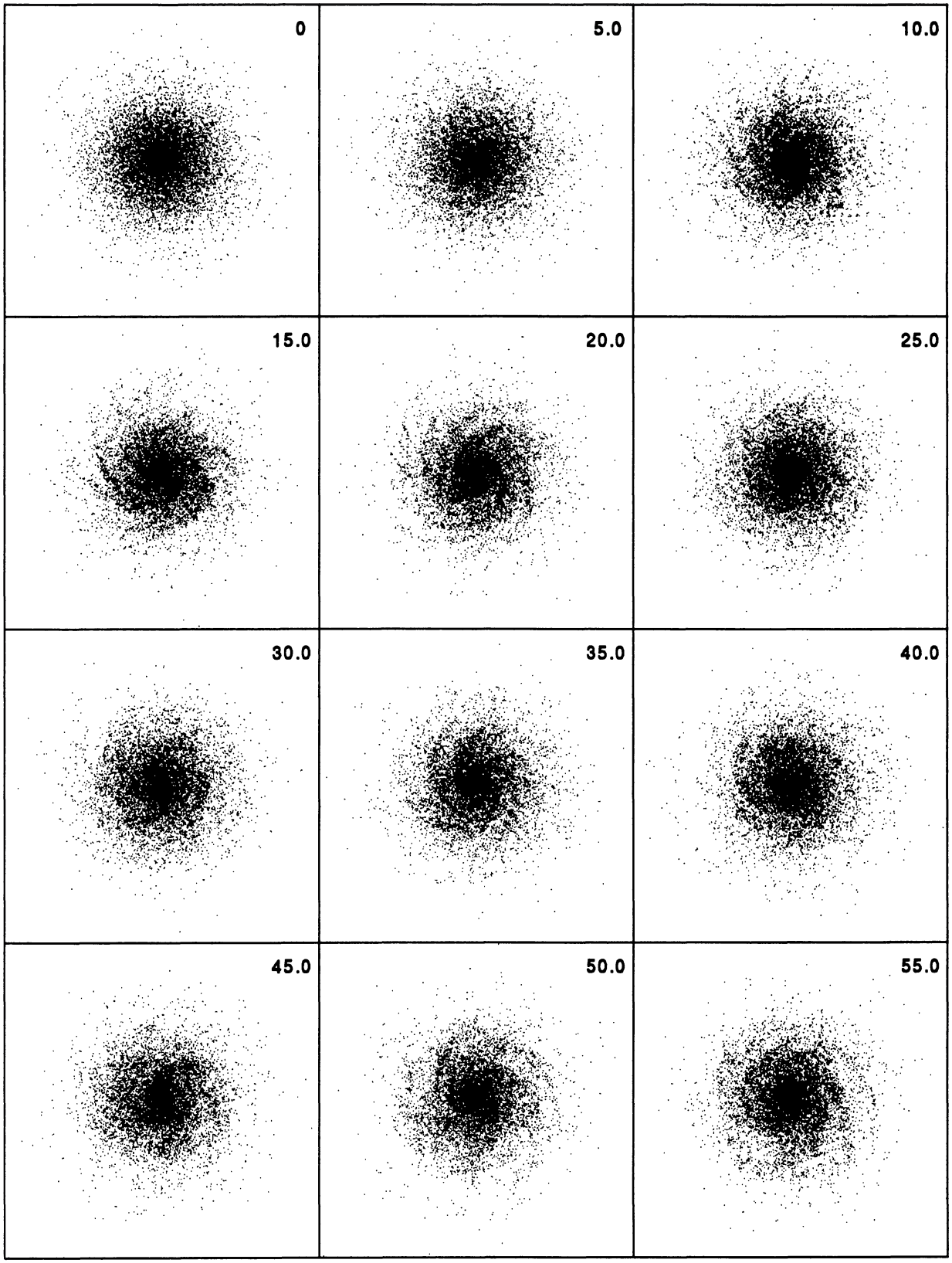

FIG. 4.—Structure arising in disk in isolated galaxy having properties described in § 3. Each frame measures 10 length units per edge, and the simulation spans ~5 rotation periods at the half-mass radius of the disk.

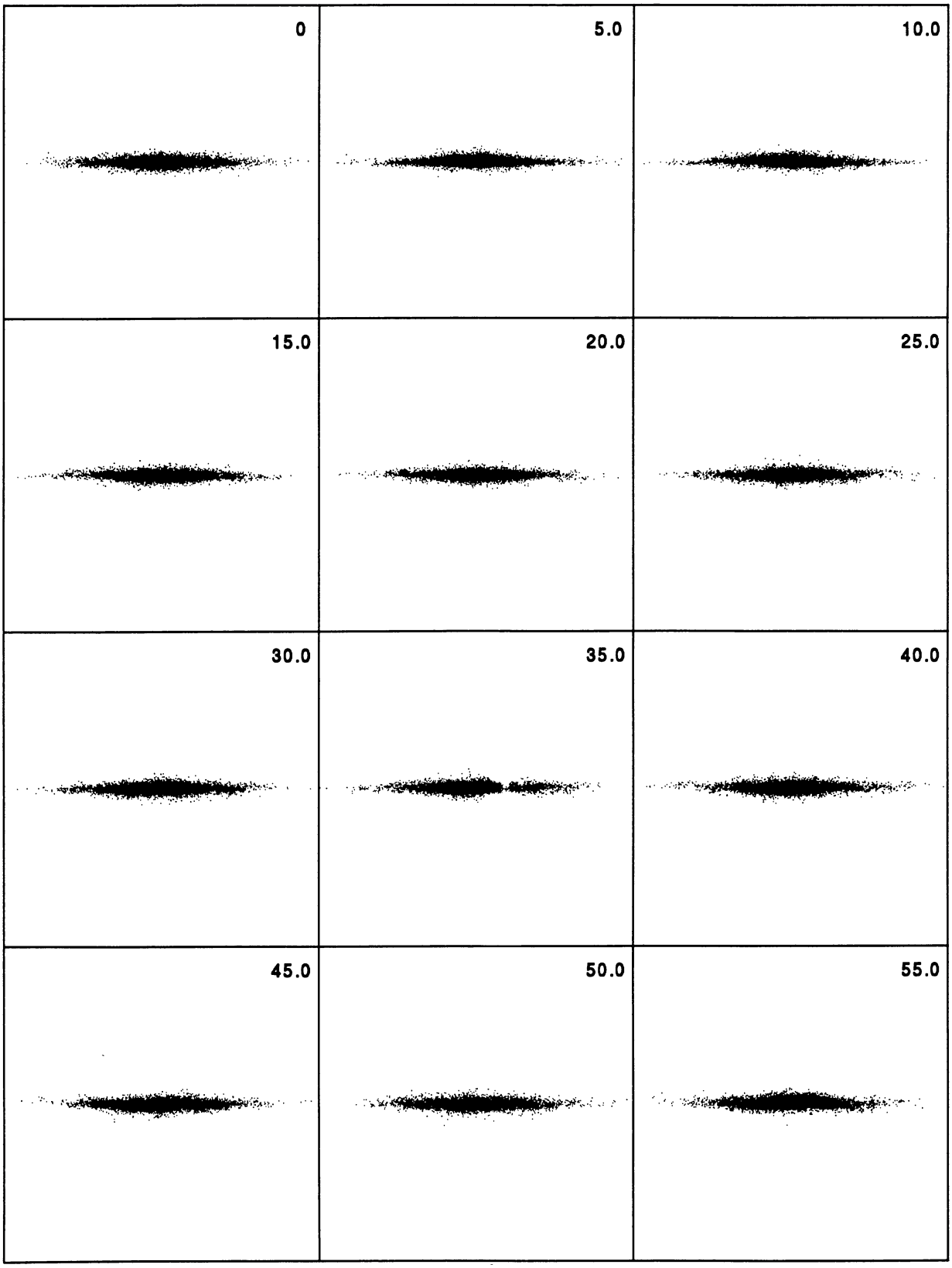

FIG. 5.—Same as Fig. 4, but viewed perpendicular to the disk plane

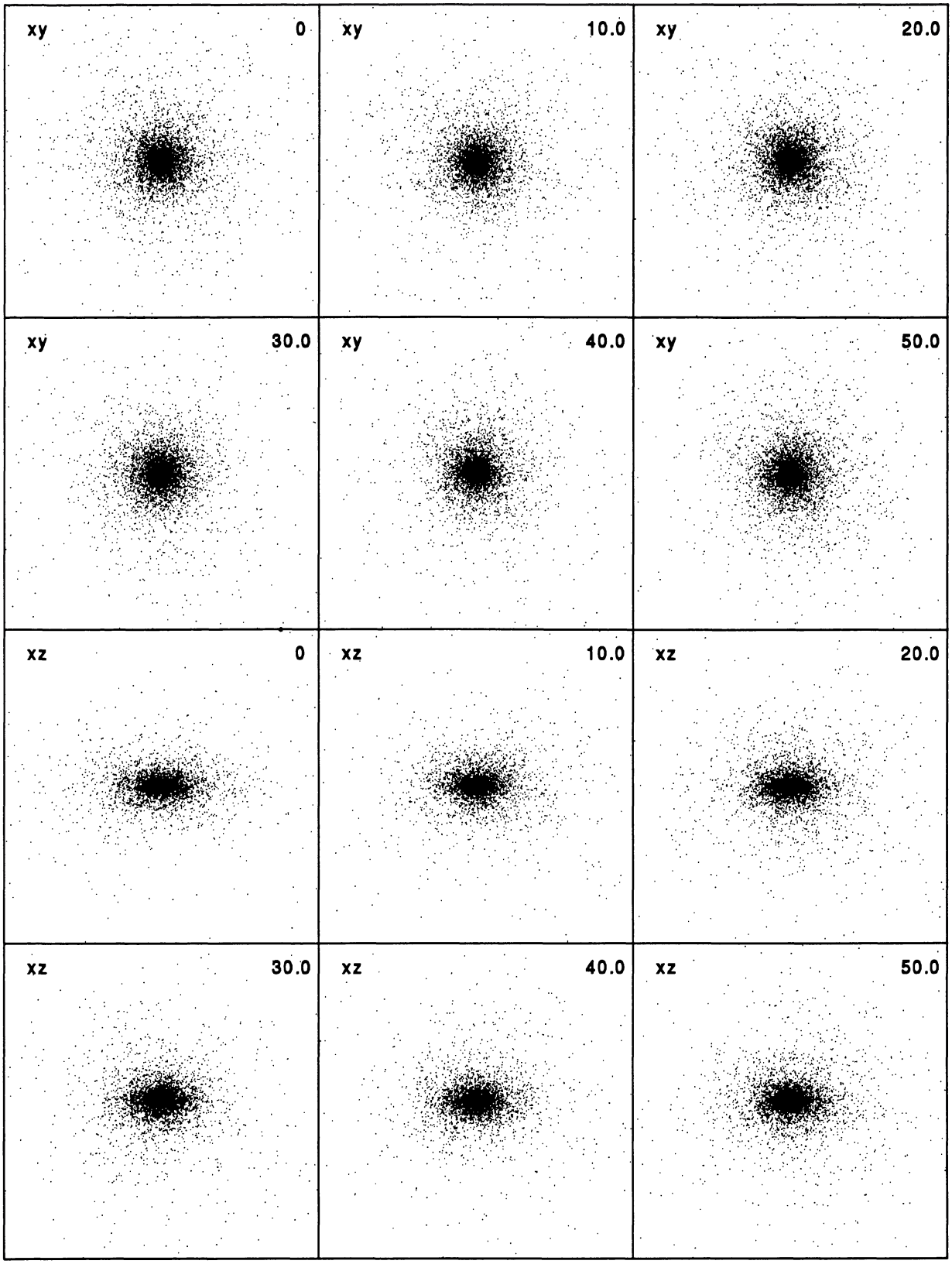

FIG. 6.—Time "evolution" of bulge component in isolated disk model. Top six panels show a view down the symmetry axis of the bulge, and bottom six panels show an orthogonal projection. Time and scales are identical to those in Figs. 4 and 5.

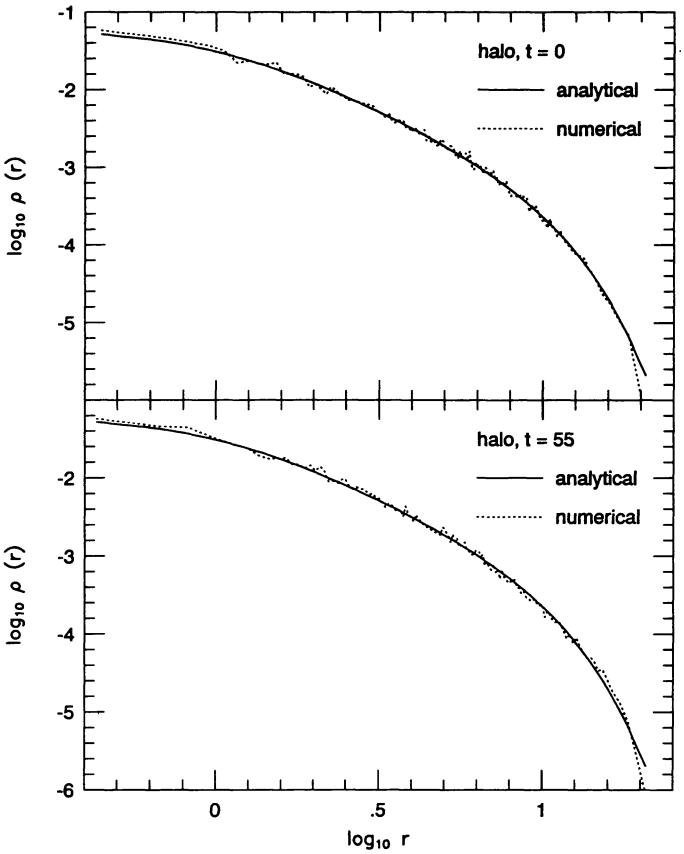

FIG. 7.—Density profile of halo component initially (*top panel*) and at the conclusion of the simulation (*bottom panel*). Dotted lines show the density measured directly from the particle distribution by binning particles in spherical shells with 128 particles per bin. Solid line shows the exact density profile, eq. (2.2).

The other properties monitored during the simulation displayed behavior consistent with that in Figures 7–10: little or no evolution immediately after the start of the calculation and only slow structural changes thereafter. These results are consistent with the interpretation that the model is nearly in equilibrium initially and evolves only gradually as the result of the numerical effects noted above.

4. CONCLUSIONS

A method for constructing N-body models of galaxies with many components has been described. In this scheme, the density field is realized exactly and the velocity field is approximated using moments of the collisionless Boltzmann equation. As demonstrated by the empirical tests here, models constructed using this technique are impressively close to equilibrium. Residual errors appear to be dominated by the Poisson noise inherent to Monte Carlo sampling.

The prescription described here can be used to systematically generate complex N-body systems that resemble actual galaxies. Numerous applications of the approach suggest themselves. For example, to date they have been used to examine the structure of remnants formed by mergers of spiral galaxies without (Hernquist 1992) and with (Hernquist 1993) bulges; the formation of shells in remnants of major mergers (Hernquist & Spergel 1992); the distribution of globular clusters in merger remnants (Hernquist & Bolte 1993); the development of spokes in ring galaxies (Hernquist & Weil 1993); the nature of violent relaxation in galaxy mergers (Spergel & Hernquist 1992); the phase-space evolution of merging galaxies (Hernquist, Heyl, & Spergel 1993); the forced response of galaxies to nonaxisymmetric perturbations associated with bars and oval distortions (Hernquist & Weinberg 1992); and effects related to ram-pressure stripping in groups and clusters (Kundic, Hernquist, & Gunn 1993).

Presently, the relatively crude implementation described here appears adequate for many of these applications. In the future, it will likely be necessary to refine the basic approach as computer hardware and software permit simulations with particle numbers significantly in excess of those discussed here. As noted in § 1, and as emphasized by S. Kent (private communication) the moment equations can be extended to increasingly high order for greater precision. The main limitation of the present algorithm lies is its inflexibility. For example, it is not well suited for constructing models whose distribution func-

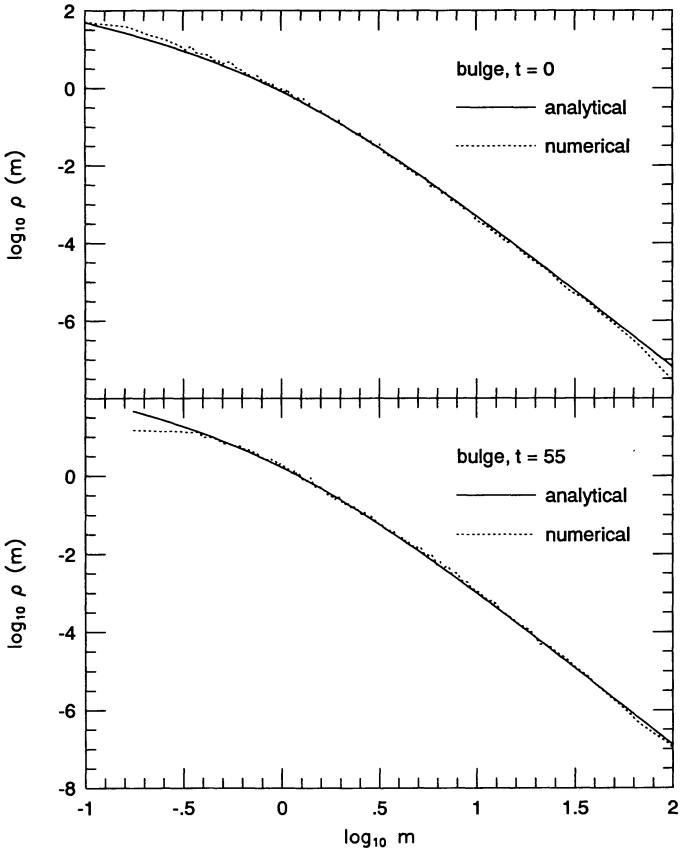

FIG. 8.—Density profile of bulge component initially (*top panel*) and at the conclusion of the simulation (*bottom panel*). Dotted lines show the density measured directly from the particle distribution by binning particles in ellipsoidal shells with 128 particles per bin. Solid line shows the exact density profile, eq. (2.6). The ellipsoidal coordinate m is defined in eq. (2.7).

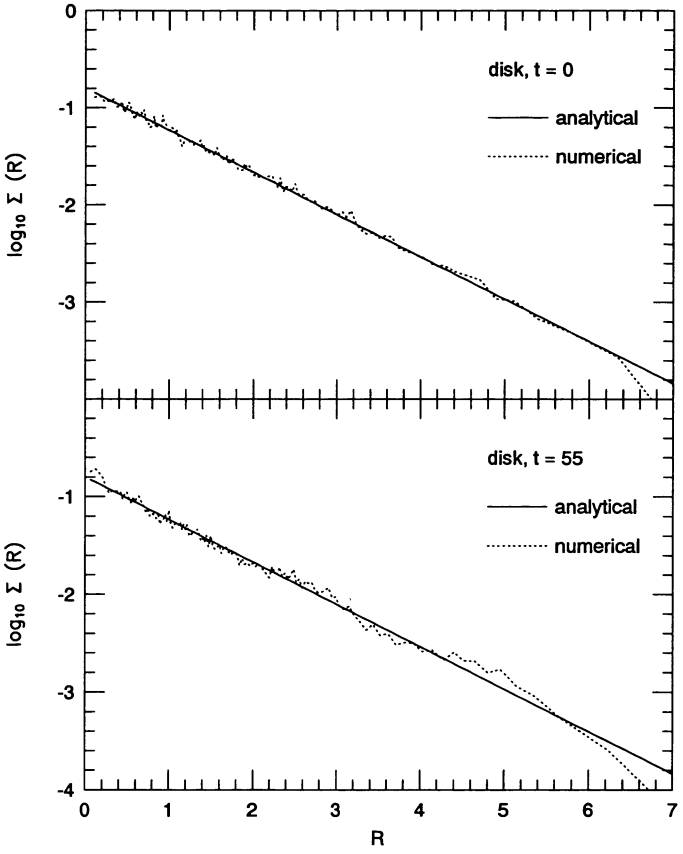

FIG. 9.—Surface density of disk component initially (*top panel*) and at the conclusion of the simulation (*bottom panel*). Dotted lines show the density measured directly from the particle distribution by binning particles in cylindrical shells with 128 particles per bin. Solid line shows the exact density profile, given by the radial dependence of eq. (2.1).

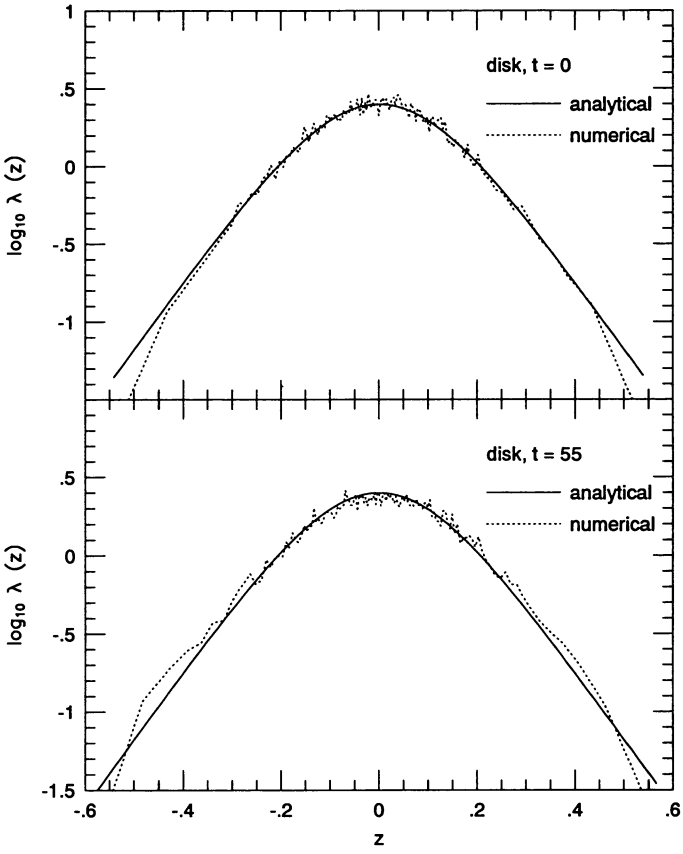

FIG. 10.—Linear density of disk component perpendicular to disk plane initially (*top panel*) and at the conclusion of the simulation (*bottom panel*). Dotted lines show the density measured directly from the particle distribution by binning particles in planes with 128 particles per bin. Solid line shows the exact density profile, given by the vertical dependence of eq. (2.1).

tions depend on more than two integrals of motion, unless some simplifications are possible, as in the case of thin disks. Thus, modeling of hot triaxial systems will likely require that some approximations be made to the distribution function or will rely on other numerical techniques, such as linear programming (Schwarzschild 1979, 1982), maximum entropy methods (Richstone 1987), or other iterative schemes (Lucy 1974).

This work was supported in part by the Pittsburgh Supercomputing Center, the Alfred P. Sloan Foundation, NASA Theory Grant NAGW-2422, and the NSF under Grant AST 90-18526 and the Presidential Faculty Fellows Program.

REFERENCES

Bahcall, J. N., & Soneira, R. M. 1980, ApJS, 44, 73
Barnes, J. E. 1988, ApJ, 331, 699
———. 1992, ApJ, 393, 484
Barnes, J. E., & Hernquist, L. 1991, ApJ, 370, L65
———. 1992, Nature, 360, 715
Barnes, J. E., & Hut, P. 1986, Nature, 324, 446
Binney, J., & Tremaine, S. 1987, Galactic Dynamics (Princeton Univ. Press)
Dejonghe, H. 1986, Phys. Rep., 133, 217
de Zeeuw, T. 1987, in IAU Symp. 127, Structure and Dynamics of Elliptical Galaxies ed. T. de Zeeuw (Dordrecht: Reidel), 271
Dubinski, J., & Carlberg, R. G. 1991, ApJ, 378, 496
Efstathiou, G., Davis, M., Frenk, C. S., & White, S. D. M. 1985, ApJS, 57, 241
Freeman, K. C. 1970, ApJ, 160, 811
Gradshteyn, I. S., & Ryzhik, I. M. 1980, Table of Integrals, Series, and Products (New York: Academic)
Hernquist, L. 1987, ApJS, 64, 715
———. 1989, Nature, 340, 687
———. 1990a, in Dynamics and Interactions of Galaxies, ed. R. Wielen (Springer: Berlin), 108
———. 1990b, ApJ, 356, 359
———. 1990c, J. Comput. Phys., 87, 137
———. 1991, Int. J. Supercomput. Appl., 5, 71
———. 1992, ApJ, 400, 460
———. 1993, ApJ, in press
Hernquist, L., & Barnes, J. E. 1991, Nature, 354, 210
Hernquist, L., & Bolte, M. 1993, ApJ, submitted

Hernquist, L., Heyl, J., & Spergel, D. N. 1993, ApJ, submitted
Hernquist, L., & Katz, K. S. 1989, ApJS, 70, 419
Hernquist, L., & Quinn, P. J. 1988, ApJ, 331, 682
———. 1989, in The Epoch of Galaxy Formation, ed. C. S. Frenk, R. S. Ellis, T. Shanks, A. F. Heavens, & J. A. Peacock (Dordrecht: Kluwer), 427
Hernquist, L., & Spergel, D. N. 1992, ApJ, 399, L117
Hernquist, L., & Weil, M. D. 1993, MNRAS, in press
Hernquist, L., & Weinberg, M. D. 1992, ApJ, 400, 80
Illingworth, G., & Schechter, P. L. 1982, ApJ, 256, 481
Kormendy, J. 1982, in Morphology and Dynamics of Galaxies, ed. L. Martinet & M. Mayor (Sauverny: Geneva Obs.)
Kormendy, J., & Illingworth, G. 1982, ApJ, 256, 460
Kundic, T., Hernquist, L., & Gunn, J. E. 1993, in preparation
Lacey, C. G., & Ostriker, J. P. 1985, ApJ, 299, 633
Lewis, J., & Freeman, K. C. 1989, AJ, 97, 139
Lucy, L. B. 1974, AJ, 79, 745
Minniti, D., White, S. D. M., Olszewski, E. W., & Hill, J. M. 1992, ApJ, 393, L47
Press, W. H., Flannery, B. P., Teukolsky, S. A., & Vetterling, W. T. 1986, Numerical Recipes: The Art of Scientific Computing (Cambridge Univ. Press)
Quinn, P. J., Hernquist, L., & Fullager, D. 1993, ApJ, 403, 74
Richstone, D. O. 1987, in IAU Symp. 127 Structure and Dynamics of Elliptical Galaxies, ed. T. de Zeeuw (Dordrecht: Reidel), 261
Schwarzschild, K. 1907, Göttingen Nachr., 614
Schwarzschild, M. 1979, ApJ, 232, 236
———. 1982, ApJ, 263, 599
Sellwood, J. A. 1989, in Dynamics of Astrophysical Disks, 155, ed. J. A. Sellwood, (Cambridge Univ. Press), 155
Spergel, D. N., & Hernquist, L. 1992, ApJ, 397, L75
Spitzer, L. 1942, ApJ, 95, 325
Toomre, A. 1963, ApJ, 138, 385
———. 1981, in The Structure and Evolution of Normal Galaxies, ed. S. M. Fall & D. Lynden-Bell (Cambridge Univ. Press), 111
Toomre, A., & Toomre, J. 1972, ApJ, 178, 623
van der Kruit, P. C., & Searle, L. 1981, A&A, 95, 105